CHINESE JOURNAL OF ANALYTICAL CHEMISTRY
Volume 42, Issue 2, February 2014
Online English edition of the Chinese language journal

Available online at www.sciencedirect.com
ScienceDirect

Cite this article as: Chin J Anal Chem, 2014, 42(2), 221–226.

RESEARCH PAPER

Characterization of *In vitro* Mineralization of Porous Poly (*L*-Lactic Acid)/Bioactive Glass Composites by Attenuated Total Reflectance-Fourier Transform Infrared Mapping

WANG Qian, JIANG Xiao-Ting, XIN Yun-Zi, CUI Jun-Xian, ZHANG Pu-Dun*
School of Science, Beijing University of Chemical Technology, Beijing 100029, China

Abstract: Attenuated total reflectance-Fourier transform infrared (ATR-FTIR) mapping was used to characterize the mineralization of porous poly (*L*-lactic acid)/ bioactive glass (PLLA/BG) composite in PBS solution. FTIR images were generated on the basis of the ratio of the absorbance of the band at 1044 cm^{-1} to the one at 1755 cm^{-1} (A_{1044}/A_{1755}) at a resolution of 8 cm^{-1} with 8-coadded scans. The imaging results showed that the amount of hydroxyapatite (HA) on the surface of the composites increased with soaking time and most of the surface area was covered by HA after being mineralized for 84 d. However, the heterogeneous mineralization increased with time lasted. The mineralization curve from the average spectra further suggested that there were four stages during mineralization. At the initial one (less than 21 d), the amounts of HA were small; at the growth one (21–70 d), BG was gradually converted to HA; at the rapid growth one (70–91 d), the mineralization was accelerated and reached up to the maximum at 91 d; and at the late stage (over 91 d), the curve became steady at first and then declined after 105 d. The results suggested that ATR-FTIR mapping was promised to be an important tool for study of the scaffold in bone tissue engineering.

Key Words: Fourier transform infrared mapping; Attenuated total reflectance; Poly (*L*-lactic acid); Bioactive glass; *In vitro* mineralization

1 Introduction

Different from other imaging techniques (e.g. electron microscopy and fluorescence microscopy), chemical imaging is used to visualize the chemical distribution of the components in a micro-domain. It contains Fourier transform infrared (FTIR) and Raman imaging. FTIR imaging appeared nearly two decades ago, and it expands FTIR technique from "point" analysis to "plane", even "stereoscopic" analysis. FTIR technique was used to study the chemical heterogeneity of a micro-region with hundreds to thousands of microns. It can be accomplished by mapping or imaging[1]. It is also suited to acquiring images for a sample with rough surface by attenuated total reflectance (ATR)-FTIR mapping[2]. FTIR imaging or mapping was applied in a number of fields, including polymers[3–6], life sciences[7,8], biomedical studies[9], archaeology[10] and forensic science[11] etc.

As a kind of bone tissue engineering material[12], bioactive glass (BG) was reported to stimulate osteogenesis *in vitro* by inducing the proliferation and osteogenic differentiation of human osteoblasts[13]. However, because of the poor processing performance, BG is usually fabricated into porous composite scaffolds by blending with natural or non-toxic synthetic polymer. Porous structure is favorable for cell growth and proliferation and for the deposition of extracellular matrix. It also facilitates the access of nutrient and oxygen and the drain of metabolites. In addition, porous composites may provide a temporary scaffold to guide the ingrowth of vascular and neural tissues[14]. When the composites are implanted into living body, BG will be gradually transformed into hydroxyapatite (HA) that is bonded strongly with bone tissue, while the polymer is gradually degraded. Due to the

Received 26 March 2013; accepted 29 September 2013
* Corresponding author. Email: zhangpd@mail.buct.edu.cn

DOI: 10.1016/S1872-2040(13)60713-6

difficulties of in vivo study, *in vitro* mineralization under the biomimetic condition is often used[15]. The *in vivo* bioactivity of the composite material can be predicted well from the *in vitro* results.

At present, the mineralization of the composite is usually characterized by scanning electron microscopy (SEM) combined with energy dispersive X-ray analysis (EDX), X-ray diffractive (XRD) analysis and infrared spectroscopy[16]. These developed methods could not show the chemical changes of compositions in a micro region, but only provide the information on changes of morphology, elemental compositions, total crystallization and total components. In this study, the changes of chemical constituents of the porous composites of poly(L-lactic acid)/bioactive glass (PLLA/BG) were systematically investigated by ATR-FTIR mapping during the *in vitro* mineralization. The changes of the morphology were also monitored by SEM.

2 Experimental

2.1 Instruments, materials and reagents

A Nexus 8700 FTIR spectrometer coupled with a Continuμm XL FTIR imaging microscope (Thermo Electron, USA) was used to acquire the FTIR maps. An S-4700 field emission scanning electron microscope (SEM, Hitachi, Japan) was used to observe the morphology changes of the materials. The mineralization experiment was conducted in a DK-420S three-way water bath (Shanghai Jinghong, China). Poly (*L*-lactide) with an inherent viscosity (η) of 1.22 dl g^{-1} and a weight-average molecular weight (M_w) of about 121000 g mol^{-1} was purchased from Jinan Daigang Biomaterials Co. Ltd. (Jinan, China). BG powder was obtained from NovaMin Technology, Inc. (FL, USA). 1,4-Dioxane, ethanol, $AgNO_3$ and all the reagents for prepared phosphate buffered saline (PBS) solution were of analytical grade.

2.2 Preparation and *in vitro* mineralization of porous PLLA/BG composites

Similar to the reference[17], solvent casting-salt leaching method was applied to prepare the porous PLLA/BG composites in this experiment. Briefly, 3 g of PLLA were dissolved with 30 mL 1,4-dioxane at room temperature, and 3 g of BG were also homogeneously suspended in another 30 mL 1,4-dioxane using an ultrasonicator. The two solutions were then mixed under vigorous magnetic stirring for 30 min. Then 24 g of ground NaCl powder with particle size of 150–250 μm (80–100 mesh) were added into mixed solution and stirred for 30 min. The as-prepared mixture was cast onto several petri dishes to a certain thickness and dried under natural conditions for 24 h. The dried slices were immersed in deionized water to remove the salt. The water was replaced every 12 h till the residual chloride ion was no longer detected (using 0.1 M $AgNO_3$ solution). Finally, the obtained porous composites were dried in a vacuum oven at 45 ºC for 48 h.

The prepared composite materials were soaked in a beaker with 250 mL PBS (pH 7.4), and then placed in a water bath at 37 ºC for mineralization. A few samples were removed every 7 d from the buffer and then were rinsed with deionized water to remove the residual PBS salts. The adsorbed water on the surface was then absorbed using filter paper and the samples were dried in a vacuum oven at 45 ºC for 24 h. The PBS solution was also replaced by the fresh one every 7 d.

2.3 ATR-FTIR mapping

After soaking in PBS for serial days, PLLA/BG samples were cut into sheets with size of 1.5 cm × 1.5 cm and fixed onto a clean glass slide which was placed on the sample stage of the imaging system. MCT detector was cooled by liquid nitrogen. Before mapping, a slide-on silicon ATR accessory fitted to a 15 × IR objective (N.A. = 0.58) was pulled out and let IR beam focus on the sample. The mapping area (100 μm × 100 μm) was thus selected and the ATR crystal was then pulled in. FTIR images were acquired at a resolution of 8 cm^{-1} in the wavenumber range of 4000–650 cm^{-1} with 8 co-added scans for samples and 64 scans for background. The acquiring, the processing and the analysis of the FTIR images were implemented using the Atlμs software of Omnic 7.2 (Thermo Electron).

2.4 Scanning electron microscopy

The dried sample was fractured after being immersed into liquid nitrogen and was fixed onto the sample stage using conductive adhesive and was then sputter-coated with Pt under high vacuum. After different mineralization days, the morphology of PLLA/BG composites was observed at 20 kV and 10 μA.

3 Results and discussion

3.1 FTIR analysis of PLLA/BG composites

In PBS solution, PLLA could be degraded into lactic acid, CO_2 and H_2O, which causing the difficulty in direct detecting PLLA, and BG could be gradually mineralized to HA[12,13], a major insoluble inorganic element ($\lg K_{sp(HA)} = -57.5$[18] at 25 °C) of human bones and teeth with high crystallinity. The micro ATR-FTIR spectra of PLLA, BG and HA are shown in Fig.1. The characteristic absorption bands of PLLA include the ones at 1755 cm^{-1} ($\nu_{C=O}$), 1184 cm^{-1} ($\nu_{as(C\text{-}O\text{-}C)}$), 1090 cm^{-1} ($\nu_{s(C\text{-}O\text{-}C)}$) and the shoulder band at 1044 cm^{-1} ($\nu_{C\text{-}CH3}$)[19]. BG is a sintered amorphous powder of several inorganic chemicals and the weak band at 1595 cm^{-1} was typical for characterisation[20]. However, the wide bands at 1460 cm^{-1}

($\nu_{as}(CO_3^{2-})$) and 1035 cm^{-1} ($\nu_{as(Si\text{-}O\text{-}Si)}$) could not be used to represent BG due to their overlapping with $\delta_{C\text{-}H}$ band of PLLA and $\nu_{P\text{-}O}$ band of HA, respectively. It is noted that the band at 1595 cm^{-1} cannot appear for each time due to BG's high activity. Fortunately, the strong absorption band at 1036 cm^{-1} ($\nu_{P\text{-}O}$) of HA is suitable for the characterization of mineralization.

3.2 ATR-FTIR images of PLLA/BG composites

The FTIR images of the non-mineralizing PLLA/BG composite are shown in Fig.2. The image at bright field is shown in Fig. 2a, in which the region of the red square is used for FTIR mapping. Figs.2b and 2c show the FTIR images based on the absorbance at 1755 cm^{-1} (A_{1755}) and the one at 1595 cm^{-1} (A_{1595}), which represent the distributions of PLLA and BG in the region, respectively. The pseudo-color represents the real absorbance distribution in the mapping area with an order of blue < cyan < green < yellow < red. Correspondingly, when cursor was placed on different sites, the spectra would also be displayed in real time. For instance, the spectra of site (d) and (e) were respectively displayed in Figs.2d and 2e. They were significantly different.

The blue area in Figs.2b and 2c, an approximate zero absorbance (as shown in Fig.2e), denoted the cavity of pore while others represented the wall of pore. These two images illustrated that the distributions of PLLA and BG in the composite were nearly identical, suggesting a homogeneous structure of the composite.

3.3 Mineralization of PLLA/BG composites by ATR-FTIR mapping

Once the PLLA/BG composites were immersed into PBS at 37 ºC, the mineralization occurred. The amount of HA increased with the mineralization process, in which PLLA was simultaneously degraded. Due to the hydrogen bonding interaction between PLLA and the yielded HA[21], the characteristic band of HA ($\nu_{P\text{-}O}$ at 1036 cm^{-1}) would shift to high frequency (*i.e.* blue shift) and overlap with the band of $\nu_{C\text{-}CH3}$, which leaded to an increase of the absorbance at 1044 cm^{-1}. Thus an absorbance ratio of the band at 1044 cm^{-1} to that at 1755 cm^{-1} ($\nu_{C=O}$ of PLLA) (A_{1044}/A_{1755}) was used to profile the FTIR image and further to visualize HA development during the mineralization. The profiled images on the basis of A_{1044}/A_{1755} were also used to eliminate the

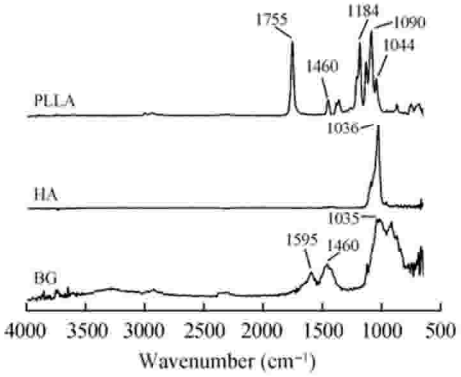

Fig.1 IR spectra of PLLA, BG and HA

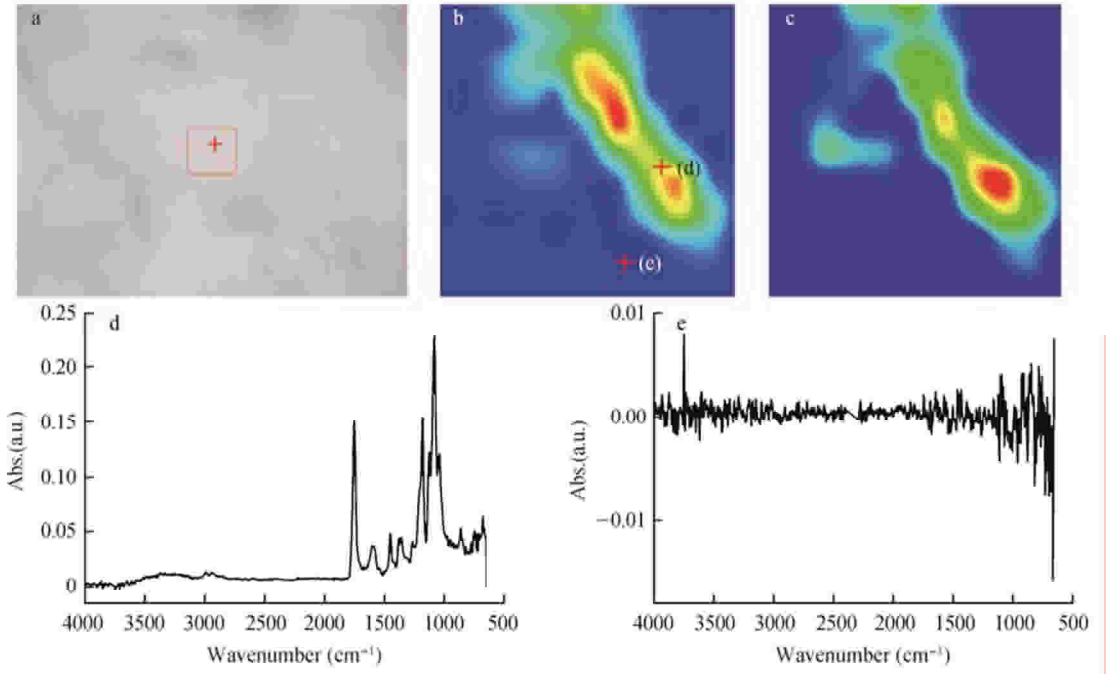

Fig.2 FTIR images of non-mineralizing PLLA/BG composite and the provided information

(a) Image at bright field; (b) and (c) FTIR images based on A_{1755} and A_{1595}; (d) and (e) are FTIR spectra at varied sites

effects of the variations of contact pressure between ATR element and different sampling points on the absorbance. The FTIR images based on absorbance ratio (Fig.3a and 3b) truly revealed the compositional variation during mineralization. However, as shown in Fig.3b, some red areas that represented the high value of the ratio were always observed in the cavity area in FTIR images after such calculation. The reason for these distortions was that the spectrum was from noise only without characteristic spectrum in these areas (Fig.2e), and the noise resulted in extremely large ratios and thus a distortion of FTIR image. Since mineralization always took place on the pore walls of composite materials, the pore wall area of each image was only chose to perform the absorbance ratio and to truly express the mineralization. As shown in Fig.4, the color of the ATR-FTIR images changed gradually from blue to red with the increase of mineralization days, suggesting that more and more HA were formed on the surface of composites. After 84 d, most of the surfaces of pore wall were covered by HA.

As times went on, FTIR images showed that the heterogeneity of mineralization increased. Figure 5 exhibits the ATR-FTIR images of the pore walls of PLLA/BG composites at different sites after mineralizing for 119 d. It is observed that there exists a large difference among the images, even at the same mineralization days. This difference was small in the early and middle stages, meaning that the mineralization was relatively homogeneous during these periods.

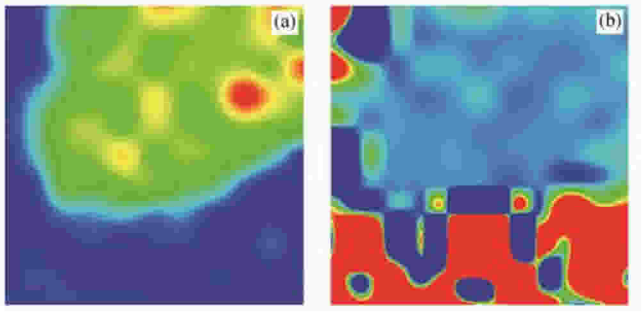

Fig.3 ATR-FTIR images of PLLA/BG composite based on (a) A_{1044} and (b) A_{1044}/A_{1755}

Red areas in (b) are actually the pores

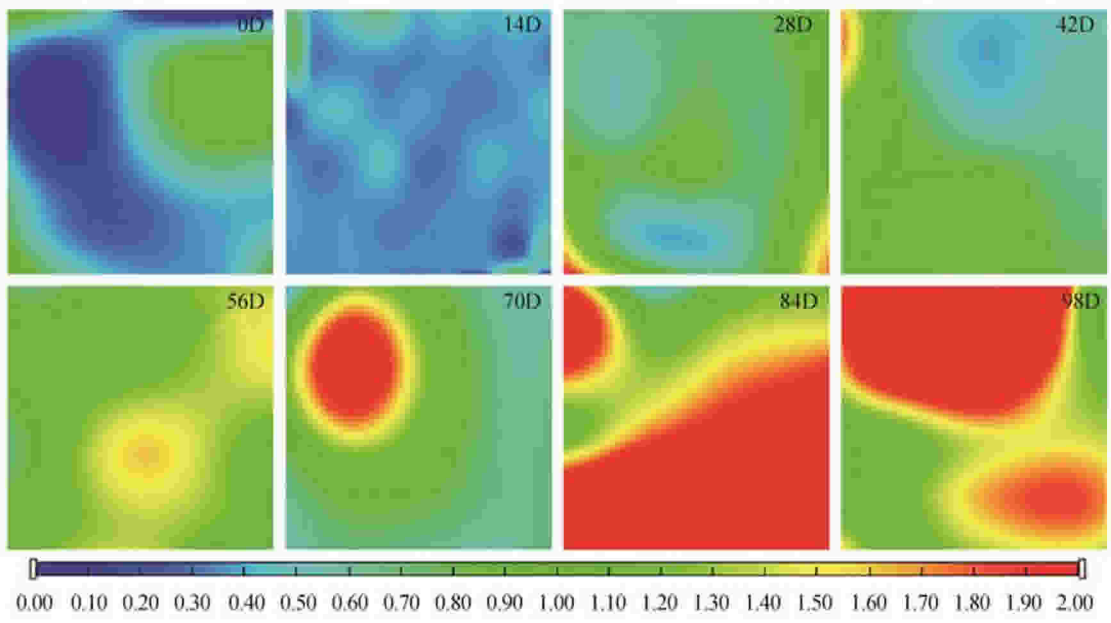

Fig.4 ATR-FTIR images of pore walls of PLLA/BG composites at different mineralization days based on the ratio of A_{1044} to A_{1755}

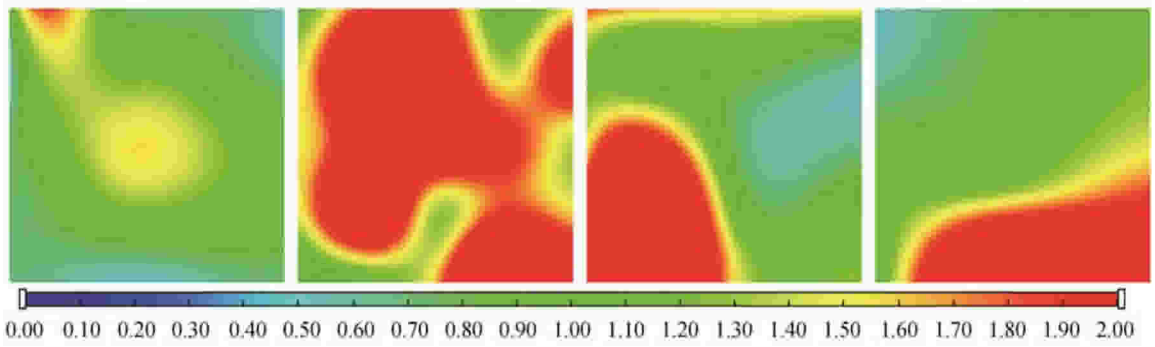

Fig.5 ATR-FTIR images of pore walls of PLLA/BG composites of different sites after mineralizing 119 d based on the ratio of A_{1044} to A_{1755}

To directly investigate the mineralization, all the spectra of each image were averaged and the curve of A_{1044}/A_{1755} based on the average ones versus the mineralization days was obtained (Fig.6). Figure 6 illustrates that there are four stages in the whole mineralization process. In the initial stage (less than 21 d), the amounts of generated HA were small and PLLA was barely degraded. In the growth stage (21–70 d), the mineralization curve went upwards, indicating that BG gradually changed to HA and PLLA began to be degraded. The mineralization was accelerated in the rapid growth stage (70–91 d) and reached up to the maximum on the 91th day, indicating that most of the surfaces of PLLA/BG composites were covered by HA during this period. However, when mineralization reached to the late stage (larger than 91 d), PBS solution would permeate into the inner of composite materials, which resulted in the degradation of PLLA at deep layer and thus the detachment of HA from surface. Since the mineralization curve comes from the statistic average of all the spectra, it is not strange that the resulting curve at this stage becomes steady at first and then declines from 105 d. This result also verified that the inhomogeneity of mineralization was increased in the late stage, as shown in Fig.5. Similar heterogeneous mineralization was also reported in other literature [22].

3.4 Characterization of *in vitro* mineralization by SEM

SEM was used to observe the morphology changes of PLLA/BG composites during mineralization. Figure 7 shows that PLLA/BG composites are obviously different from each other at different stages. Before mineralization (0 d), no HA crystal was observed on the pore walls of the composite material. After soaking in PBS for 21 d (*i.e.* in the initial stage), a few needle-like aggregates of HA were observed. More HA crystals were found in the SEM image after mineralizing 63 d (*i.e.* in the growth stage). HA crystals were significantly increased after 84 d (*i.e.* in the rapid growth period) and the structure of the crystal was gradually transformed into a network structure (Fig.7, 84 d). This structure became more obvious in the late stage (105 d) than in the rapid one, and it was suitable to increase the strength of the porous composite materials. The results indicated that both the chemical composition and the morphology of the porous PLLA/BG composite were changing during *in vitro* mineralization process.

4 Conclusions

ATR-FTIR mapping was used to characterize the *in vitro* mineralization of PLLA/BG composites. Compared with images based on the absorbance of single band, the ones based on the absorbance ratio (A_{1044}/A_{1755}) could truly reflect the generation of HA during mineralization. The mapping results indicated that the amounts of HA on the surfaces of the composites increased with soaking time and most of the surface area were covered by HA after being mineralized for 84 d. However, as mineralization went on, the heterogeneous mineralization increased. The mineralization curve revealed that the mineralization was accelerated after 70 d and reached up to the maximum at 91 d. After 91 d the curve became steady at first and then declined after 105 d. The results suggested that ATR-FTIR mapping was quite feasible for the study of the scaffold in bone tissue engineering.

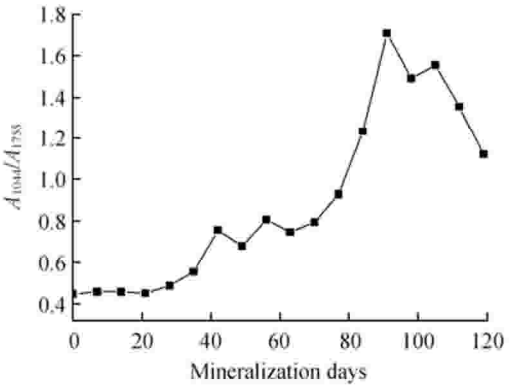

Fig.6 Curve of A_{1044}/A_{1755} of the average spectra versus the mineralization days

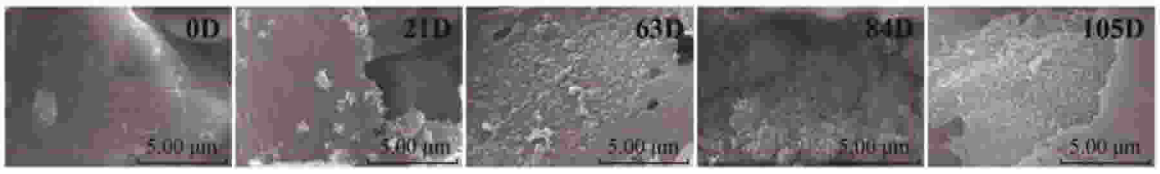

Fig.7 SEM images of PLLA/BG composites after mineralizing 0, 21, 63, 84 and 105 d

References

[1] Bhargava R, Wall B G, Koenig J L. *Appl. Spectrosc.*, **2000**, 54: 470–479

[2] Kazarian S G, Chan K L A. *Appl. Spectrosc.*, **2010**, 64: 135A–152A

[3] Zhou X, Zhang P D, Jiang X T, Rao G Y. *Anal. Sci.*, **2007**, 23 (7): 877–880

[4] Zhou X, Zhang P D, Jiang X T, Rao G Y. *Vib. Spectrosc.*, **2009**, 22(1): 17–21

[5] Zheng A G, Zhao Y, Xu Y Z, Wang D J, Zhang X Q, Zhou Y, Weng S P, Wu J G, Xu R F. *Spectroscopy and Spectral Analysis*, **2004**, 24(7): 803–805

[6] Zhou Y M, Li B B, Zhang P D. *Appl. Spectrosc.*, **2012**, 66(5):

566–573

[7] Hackett M J, Lee J, El-Assaad F, McQuillan J A, Carter E A, Grau G E, Hunt N H, Lay P A. *ACS Chem. Neurosci*., **2012**, 3: 1017–1024

[8] Beljebbar A, Dukic S, Amharref N, Bellefqih S, Manfait M. *Anal. Chem.*, **2009**, 81(22): 9247–9256

[9] Chan K L A, Kazarian S G, Vassou D, Gionis V, Chryssikos G D. *Vib. Spectrosc.*, **2007**, 43: 221–226

[10] Mazzeo R, Joseph E, Prati S, Millemaggi A. *Anal. Chim. Acta*, **2007** 599(1): 107–117

[11] Ricci C, Bleay S, Kazarian S G. *Anal. Chem.*, **2007**, 79(15): 5771–5776

[12] Rahaman M N, Day D E, Bal B S, Fu Q, Jung S B, Bonewald L F, Tomsia A P. *Acta Biomater.*, **2011**, 7: 2355–2373

[13] Jones J R. *Acta Biomater.*, **2013**, 9: 4457–4486

[14] Armentano I, Dottori M, Fortunati E, Mattioli S, Kenny J M. *Polym. Degrad. Stabil.*, **2010**, 95: 2126–2146

[15] Varila L, Fagerlund S, Lehtonen T, Tuominen J, Hupa L. *J. Eur. Ceram. Soc.*, **2012**, 32(1): 2757–2763

[16] El-Kady A M, Saad E A, El-Hady B M A, Farag M M. *Ceram. Int.*, **2010**, 36: 995–1009

[17] Jiang X T, Wang Q, Zhang P D. *Chemical Research and Application*, **2011,** 23(6): 755–760

[18] Oliva J, Cama J, Cortina J L, Ayora C, De Pablo J. *J. Hazard. Mater.*, **2012**, 213-214: 7–18

[19] Nejati E, Firouzdor V, Eslaminejad M B, Bagheri F, *Mater. Sci. Eng. C,* **2009**, 29: 942–949

[20] Kazarian S G, Chan K L A. *Biomaterials*, **2004**, 25: 3931–3938

[21] Zhou S, Zheng X, Yu X, Wang J, Weng J, Li X, Feng B, Yin M. *Chem. Mater.*, **2007**, 19(2): 247–253

[22] Murphy W L, Mooney D J, *J. Am. Chem. Soc.*, **2002**, 124(9): 1910–1917